Mn_2FeWO_6: A New Ni_3TeO_6-Type Polar and Magnetic Oxide

*Man-Rong Li, Mark Croft, Peter W. Stephens, Meng Ye, David Vanderbilt, Maria Retuerto, Zheng Deng, Christoph P. Grams, Joachim Hemberger, Joke Hadermann, Wen-Min Li, Chang-Qing Jin, Felix O. Saouma, Joon I. Jang, Hirofumi Akamatsu, Venkatraman Gopalan, David Walker, and Martha Greenblatt**

Polar magnets are one of the most promising materials for multiferroics and spintronics. Recently, the $A_2BB'O_6$-type corundum derivatives have drawn much interest due to their remarkable magnetic and electronic properties with polar structures and multiferroic and second harmonic generation (SHG) behavior.[1–6] These structures are related to perovskite, but unlike perovskites, which have corner-sharing B site octahedra, in these phases, with unusually small A-site cations, both the A and B sites are octahedrally coordinated. The corner-, face-, and edge-sharing octahedra form a 3D lattice.[2,7] The $A_2BB'O_6$-type corundum derivatives can crystallize in the centrosymmetric ilmenite (IL, space group *R*-3), or in non-centrosymmetric $LiNbO_3$ (LN, *R*3*c*), or ordered ilmenite (OIL, *R*3), or Ni_3TeO_6 (NTO, *R*3) structure, as shown in Figure S1 (Supporting Information). The stabilization of any one of these structures depends on the cation arrangement and their ordering/disordering degree, which are affected by the cationic size and charge differences, electron configuration, and synthesis conditions.[1,8–11] The general structural features of $A_2BB'O_6$-type corundum derivatives with octahedral coordination of all metal sites favor the formation of practical magnetic and multiferroic/magnetoelectric materials by incorporation of magnetic transition metal ions. Recently, near room temperature (RT) ferrimagnetic (FiM) behavior of Mn_2FeSbO_6 ($T_C \approx 270$ K)[1] and antiferromagnetic (AFM) Ni_3TeO_6 with nonhysteretic colossal magnetoelectricity[4] were reported. More recently, we reported on AFM and pyroelectric Mn_2FeMO_6 (M = Nb and Ta)[3] and Zn_2FeTaO_6[2] phases with $T_N \approx 90$ and 22 K, respectively, and short-range magnetic interactions up to 210 K. We showed above-RT FiM ($T_C \approx 337$ K) and semiconductor behavior in Mn_2FeMoO_6, where a unique magnetic structure stabilized polarization.[6]

In this work, we present the high pressure and temperature (HPT) synthesis of Mn_2FeWO_6—a new magnetic and polar member of the $A_2BB'O_6$-type corundum derivative family, and the results of the crystal structure, SHG activity, magnetic phase diagram, and electrical/dielectric properties. First-principles calculations are also carried out to better understand its structure, polarization, complex magnetic properties, and to point to new materials design with multifunctional properties.

Polycrystalline black Mn_2FeWO_6 was prepared at 1673 K for 1 h at 8 GPa. Original lab powder X-ray diffraction (PXD, Figure S2, Supporting Information) indicates a rhombohedral cell ($a \approx 5.3$ Å, $c \approx 13.9$ Å) of the main phase and a small wolframite impurity (Figure S3a,b and Table S1, Supporting Information). **Figure 1**a presents the RT synchrotron powder X-ray diffraction (SPXD) patterns of Mn_2FeWO_6, which could correspond to any of the *R*3 or *R*-3 structure types discussed above. However, the high-angle annular dark field scanning transmission electron microscopy (HAADF-STEM) images (Figure 1b and S4, Supporting Information) clearly show Fe/W ordering, and thus rule out IL prototype for Mn_2FeWO_6.

Dr. M.-R. Li, Dr. M. Retuerto, Dr. Z. Deng, Prof. M. Greenblatt
Department of Chemistry and Chemical Biology
Rutgers, the State University of New Jersey
610 Taylor Road, Piscataway, NJ 08854, USA
E-mail: martha@chem.rutgers.edu

Prof. M. Croft, M. Ye, Prof. D. Vanderbilt
Department of Physics and Astronomy
Rutgers, the State University of New Jersey
136 Frelinghusen Road, Piscataway, NJ 08854, USA

Prof. P. W. Stephens
Department of Physics & Astronomy
State University of New York
Stony Brook, NY 11794, USA

Dr. C. P. Grams, Prof. J. Hemberger
II. Physikalisches Institut
Universität zu Köln
D-50937 Köln, Germany

Prof. J. Hadermann
EMAT, University of Antwerp
Groenenborgerlaan 171, B-2020 Antwerp, Belgium

W.-M. Li, Prof. C.-Q. Jin
Institute of Physics
Chinese Academy of Sciences
P. O. Box 603, Beijing 100080, China

F. O. Saouma, Prof. J. I. Jang
Department of Physics
Applied Physics and Astronomy
Binghamton University
P.O. Box 6000, Binghamton, NY 13902, USA

Dr. H. Akamatsu, Prof. V. Gopalan
Department of Materials Science and Engineering
Pennsylania State University
University Park, PA 16802, USA

Prof. D. Walker
Lamont Doherty Earth Observatory
Columbia University
61 Route 9W, PO Box 1000, Palisades, NY 10964, USA

DOI: 10.1002/adma.201405244

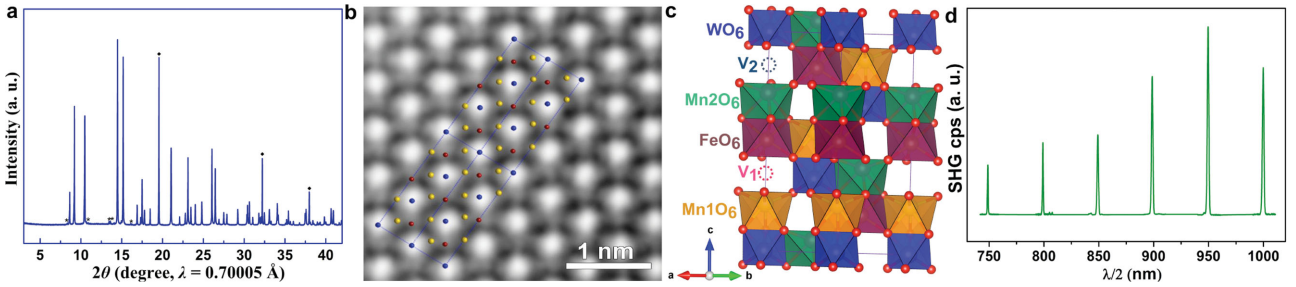

Figure 1. a) SPXD patterns of Mn_2FeWO_6 collected at RT, where the asterisks (*) and diamonds (♦) denote the peaks of a small wolframite impurity and diamond internal standard, respectively. b) A close up HAADF-STEM image of Mn_2FeWO_6 projected along [100]. The projected structure model is added, with W-blue, Mn-yellow, Fe-Red. c) The crystal structure of Mn_2FeWO_6 with FeO_6 and WO_6 polyhedral presentation of the B-sublattice viewed along [110] direction. The dashed circles indicate the centroids of octahedral vacancies along the *c*-axis between $Mn1O_6$ and FeO_6 (marked as V_1) and $Mn2O_6$ and WO_6 (V_2). $Mn1O_6$, orange yellow; $Mn2O_6$, dark green; FeO_6, brown; WO_6, blue; O, red spheres. d) Wavelength-dependent SHG response of Mn_2FeWO_6 at RT.

The cation ordering in Mn_2FeWO_6 is further supported by the SPXD data refinements, since unacceptable fitting was obtained in the IL structure model (R_p/R_{wp} = 13.35/18.36%). Although the data show comparable fittings in OIL (R_p/R_{wp} = 5.16/6.50%) and NTO (R_p/R_{wp} = 5.01/6.33%, Figure S5, Supporting Information) models, the OIL structure can be easily excluded due to the unreasonable atomic displacement parameters and bond valence sum (BVS) values,[12] which leave the NTO structure as the only solution. The amount of wolframite-type (Mn,Fe)WO_4 impurity phase is estimated to be ≈1.63 wt%.[13] The refined structural parameters are listed in Table S2 (Supporting Information). The atomic occupancies were fixed to unity since refining them only leads to small deviations (less than 1%), which suggests that the slightly Fe-poor part was only formed in a very small area of the sample surface (Figure S3a, Supporting Information). No Fe/W disordering and oxygen defects were detected within the standard deviations during the refinements. It is meaningless to discern any possible Mn/Fe disordering due to their very similar X-ray scattering effects.

The NTO-type crystal structure of Mn_2FeWO_6 has the highest cation ordering degree among the $A_2BB'O_6$-type corundum derivatives we have studied thus far.[6,8] The structure contains two crystallographically distinct Mn (Mn1 and Mn2) at the A-sites, ordered Fe and W on the B- and B′-sites, and two independent oxygen atoms (O1 and O2) (Figure 1c and Table S2, Supporting Information). The corner-sharing FeO_6 and WO_6 octahedral B-sublattice interconnects with the similar corner-sharing $Mn1O_6$ and $Mn2O_6$ A-sublattice via face-sharing pairs ($Mn1O_6/WO_6$ and $Mn2O_6/FeO_6$) along the *c*-axis and edge-sharing pairs ($Mn1O_6/FeO_6$ and $Mn2O_6/WO_6$) in the *ab*-plane, forming a 3D network structure.[2] Selected metal-oxygen bond lengths and angles are listed in Table S3 (Supporting Information). Due to electrostatic repulsions, atoms at the octahedral sites of the face-sharing octahedral pairs displace away from each other along the *c*-axis towards the octahedral vacancies below and above (V_1 and V_2 in Figure 1c), which leads to exceptionally large atomic displacements (*ds*) from their octahedral centroids (d_{Mn1} = 0.449(3) Å, d_W = 0.220(3) Å, d_{Mn2} = 0.544(2) Å, and d_{Fe} = 0.126(6) Å) comparable to other corundum-related analogs.[2,6] These anisotropic atomic displacements in Mn_2FeWO_6 (as reflected by the distortion parameters (Δ)[14] in Table S3, Supporting Information) give three long and three short metal oxygen bonds for each octahedron. The structural polarization of Mn_2FeWO_6 is directly confirmed by SHG measurements at RT (Figure 1d) and down to 10 K (Figure S6, Supporting Information). The average <Mn–O> bond lengths of Mn1 (2.187(9) Å) and Mn2 (2.228(6) Å) are closely comparable with those in other corundum-derivative analogs (Table S4, Supporting Information). The average <Fe–O> distance (2.154(10) Å) is somewhat longer than that in the isostructural $Mn_2^{2+}Fe^{3+}Mo^{5+}O_6$ (2.033(4) Å), which suggests that the formal cation oxidation states of $Mn_2^{2+}Fe^{2+}W^{6+}O_6$, are consistent with the corresponding BVS calculations (Table S3, Supporting Information)[12] and X-ray absorption near-edge spectroscopy (XANES) results (Figure S7, Supporting Information). With the point-charge displacement model,[15] we obtained a relativley large spontaneous polarization (P_S) of 59.5 μC cm^{-2} along the *c*-axis, comparable with the values reported for other corundum-related phases such as $ZnSnO_3$ (58 μC cm^{-2}),[16,17] $LiNbO_3$ (67 μC cm^{-2}),[18] Zn_2FeTaO_6 (50 μC cm^{-2}),[2] and Mn_2FeMoO_6 (68 μC cm^{-2}).[6] A definition that is more closely related to a hypothetical switchable polarization[16] will be discussed in the theory section below. Compared with other Mn_2FeMO_6 (M = Sb^{5+}, Nb^{5+}, Ta^{5+}, Mo^{5+}, and W^{6+}) analogs (Table S4, Supporting Information),[19] it appears that the preferred stability of W^{6+}/Fe^{2+} oxidation states, the larger size and charge difference between octahedral W^{6+} and Fe^{2+}, and their full ordering on the B sites, are responsible for the NTO-type structure of Mn_2FeWO_6.

Magnetization (*M*) versus temperature (*T*, 2 to 400 K) and field (0.01 to 14 T) for Mn_2FeWO_6 are shown in **Figure 2**. Figure 2a shows the logarithmic-*M* versus *T* curves collected in the field-cooled (FC) and zero-field-cooled (ZFC) modes (linear *M* (*T*) and d*M*/d*T* curves can be seen in Figure S8a, Supporting Information). Note that the small high-*T*, low-*H*, B-anomaly (≈340 K), and FC/ZFC disparity is due to a trace magnetic impurity phase other than wolframite (Figure S9, Supporting Information) as confirmed by the specific heat measurements and will be neglected hereafter. The positive portion of full magnetization versus field (*M*(*H*)) loops is shown in Figure 2b with selected full *M*(*H*) loops shown in Figures S8b (Supporting Information).

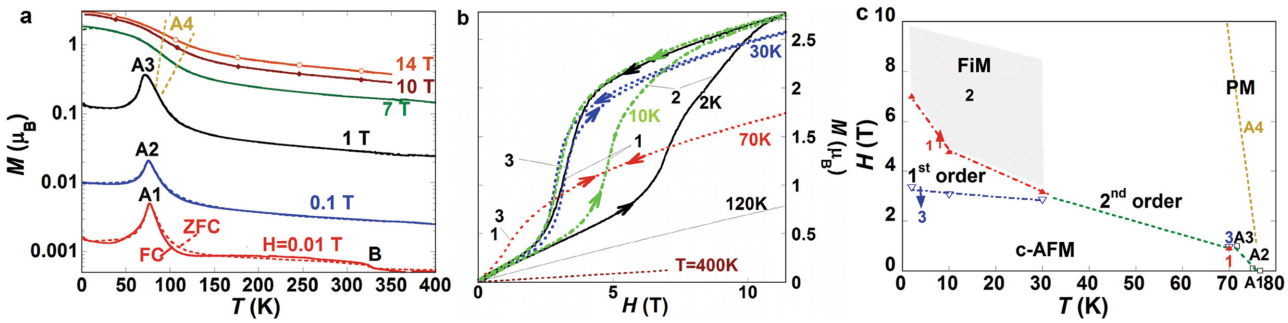

Figure 2. a) A logarithmic plot of the magnetization (M) versus temperature (T) curves at a series of fields between 0.01 and 14 T. The ZFC and FC curves, respectively, are dashed and solid at each field. Note the A1-A3 peak features are labeled along with the very low-field B step feature. b) The positive portion of magnetization loops, $M(H)$, where the labels 1, 2, and 3 correspond to the features identified in the phase diagram. c) A schematic magnetic H–T phase diagram inferred from features in the $M(H,T)$ curves in (a,b), and Figure S10 (Supporting Information) along with the band structure results. The labels 1, 2, 3, B, A1, A2, A3, and A4 correspond to the features identified in these figures and the text. The red-1 and blue-3 lines are, respectively, the locus of metastability limits under increasing and decreasing field, respectively, for a field-induced first-order transition. The green line indicates a second-order transition from the collapse of hysteresis and the inflection point in the $M(H)$ curve at 70 K. The A1, A2, and A3 indicate second-order transitions in the $M(T)$ curves. The A4 region comes from the negative peaks in the $dM(T)/dT$ curves in Figure S8a (Supporting Information). In the gray-2 crosshatched region, the increasing field magnetization curves (a) show a continuous increase of magnetization.

At and below $H = 1$ T, the $M(T)$ results in Figure 2a clearly manifest sharp peak features (A1-A2-A3) at ≈70 K, typical of a robust AFM-type order. The $M(H)$ results presented in Figure 2b strongly support this conclusion with the robust magnetic $M(H)$ hysteresis loop at $T = 2$ K, most dramatically evidencing a first-order increasing-field-induced transition out of the AFM state. The density functional theory (DFT) calculations (see below) suggest that the the $H = 0$ ordered state is a complex, two cell AFM state (c-AFM), while the field-induced ordered phase is a FiM state with a larger net moment. In Figure 2b, following the increasing field (from $H = 0$), $T = 2$ K, $M(H)$ curve, one sees a rapid rise in the 7–10 T range suggesting a field suppression of the assumed c-AFM order parameter. With decreasing field (again at $T = 2$ K), the magnetization evidences a rapid restoration of c-AFM order parameter in the 4–2 T range. This hysteretic suppression–restoration of the c-AFM order indicates a first-order field-induced phase transition. In a powdered material, the crystalline anisotropies of this transition are averaged. The c-AFM order suppression with increasing field is seen to be a two-step process (note features 1 and 2).

The $T = 10$ K, $M(H)$ curve in Figure 2b shows a much shrunk hysteresis loop with the largest change in the critical field for the increasing field part of the loop (≈4–5 T). The $T = 30$ K, $M(H)$ loop manifests only a small hysteresis. Again the increasing field transition has moved down strongly, whereas the decreasing field transition remains little varied. In the $T = 70$ K curve, the hysteresis appears to have vanished; however, there is still a field-induced inflection point more typical of a second-order, continuous transition (labeled with 1 and 3 in the figure). The 120 K $M(H)$ curve shows no evidence for this robust transition.

The low-temperature magnetic phase diagram in Figure 2c incorporates the various low-temperature magnetic features discussed above. The robust thermal anomalies (A1-A2-A3) in the $M(T)$ curves in Figure 2b show the slow field-induced suppression of the c-AFM ordering temperature. The field-induced continuous transition at $T = 70$ K agrees well with the thermal anomaly A3 for the nominal second-order AFM phase boundary. At temperatures between 2 and 30 K, the increasing field c-AFM suppression (1-red line) and the decreasing field c-AFM order restoration (3-blue line) are indicative of the first-order transition. The hysteresis of this first-order transition shrinks and the 1-red and 3-blue metastability limit curves come together someplace in the range above 30 K. Thus, the passage from a first- to a second-order transition is indicated. It is assumed that the first-order, field-induced transition, below ≈30 K, is into the FiM phase and is indicated by the gray-hashed H-T range (labeled 2 in Figure 2c). In this polycrystalline sample, the distribution of the magnetic c-axis anisotropy direction, with respect to the external magnetic field, would be expected to leave untransformed c-AFM domains in the highest field region.

The negative peak in the higher field dM/dT curves (See A4 region in Figure S8a, Supporting Information) indicates the temperature range for the continuous onset of AFM correlations in the paramagnetic (PM) phase and is indicated by the A4 region in the phase diagram (Figure 2c). The energy scale of this onset is correlated with the $H = 0$, c-AFM phase transition. The temperature induced collapse of the high-field FiM phase is uncertain; however, it presumably lies lower than the A4 region and higher than the two-shaded region. Noting that the low-temperature limit of the 14 T $M(T)$ curve is just ≈3 μ_B and that the high-field slope of the $T = 2$ K $M(H)$ curve is a sizable 0.07 μ_B/T (far from saturation), it appears that a saturated PM state has not been achieved in the highest fields and lowest temperatures studied.

To better understand the crystal structure and magnetic and electric properties, first-principles calculations were carried out. The nominal d^5 electronic configuration of Mn^{2+}, d^6 of Fe^{2+}, and d^0 of W^{6+} is confirmed by the DFT + U spin-polarized calculations, which predict magnetic moments of about 4.6 μ_B on each Mn and 3.7 μ_B on each Fe, consistent with the high-spin $S = 5/2$ and $S = 2$ configurations on Mn and Fe, respectively. A small magnetic moment of about 0.1 μ_B is induced on W as a result of covalent effects. To investigate the magnetic structure of Mn_2FeWO_6, four different types of unit cell were studied,

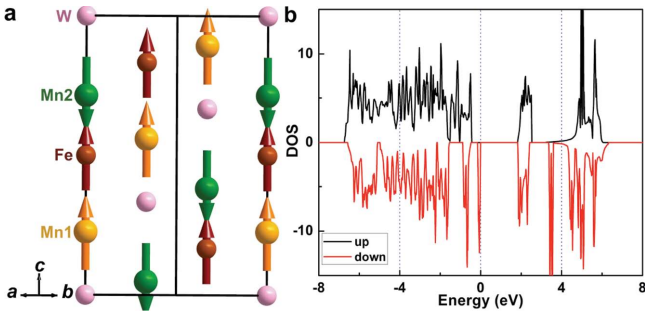

Figure 3. a) The ground FiM *udu* state of single-cell Mn_2FeWO_6 slab structure with Mn2 moments antiparallel to both Mn1 and Fe moments. b) A plot of the DOS in the *udu* magnetic structure of Mn_2FeWO_6, showing insulating behavior with a bandgap of 1.83 eV.

each containing a single formula unit and with a collinear magnetic structure. We adopt a notation like "*udu*" to describe the possible spin structures, where "*u*" is spin-up, "*d*" is spin-down, and the spins are given on Mn1, Mn2 and Fe, in that order. The four possible states (not counting those that are trivially related by a global spin reversal) are *uuu*, *uud*, *udu*, and *udd*, as listed in Figure S10 and Table S5 (Supporting Information). Of these, the FiM *udu* structure, with Mn2 moments antiparallel to both Mn1 and Fe moments, is found to be the ground state (**Figure 3**a) in the RT structure from SPXD analysis. The DFT structural parameters for *udu* ordering are listed in Table S2 (Supporting Information). The net magnetic moment in the *udu* ordering is 4 μ_B/f.u., which is larger than the measured moment of ≈3 μ_B/f.u. at 14 T (Figure 2b and S8, Supporting Information), suggesting that the moment may not saturate until a higher field, as discussed above. A plot of the density of states (DOS) in the *udu* magnetic structure, presented in Figure 3b, shows that the *udu* state is insulating with a bandgap of 1.83 eV, and the valence band maximum (VBM) is composed mainly of Fe 3*d* orbital character.

In order to extract the P_S of the *udu* structure, we define it to be half the change of Berry-phase polarization that would occur if the polarization were reversed by moving the Mn atoms through the O planes into empty octahedral sites, similar to the polarization reversal path of $LiNbO_3$. We obtain P_S = 67.8 μC cm^{-2}, which is, perhaps accidentally, comparable with the value of 59.5 μC cm^{-2} estimated from the point-charge displacement model. Our calculations suggest that the optimal switching path occurs via the sequential transfer of Mn2 and then Mn1 across the O plane, but we find that intermediate structure is metallic due to a change in Fe *d*-orbital ordering. This metallic character probably defeats any attempt at polarization reversal, helping to explain the absence of ferroelectric switching in the dielectric and polarization measurements (Figure S11, Supporting Information).

We also used first-principles calculations to consider doubled-cell magnetic structures containing two formula units as possible candidates for the observed low-temperature AFM magnetic structure seen at zero field. The results are presented in Table S6 (Supporting Information). With the unrelaxed experimental ion coordinates, the lowest-energy magnetic ordering among the doubled-cell configurations is *uud–ddu*, i.e., the one obtained by a combination of *uud* and *ddu* primitive cells. After relaxation of the internal coordinates, however, the *udu–udd* magnetic structure becomes the most stable. The energy reduction from lattice relaxation is largest for the *udu–udd* composite cell because the magnetic ordering of the two subcells is not related by time-reversal symmetry, so that additional zone-boundary phonon modes can relax and contribute to lowering the energy. The *udu–udd* double cell is even lower in energy than the *udu* single-formula-unit structure, by 13 meV/f.u. Our results suggest that the magnetic double-hysteresis loop visible at low temperature in Figure S8b (Supporting Information) might be understood as a series of transitions from a *dud* FiM ordering at negative field to a *udu–udd* (or *dud–duu*) configuration at zero field, then back to a *udu* FiM configuration at positive field. We have only considered collinear magnetic structures here. However, our study of the doubled-cell structure strongly suggests that there is a magnetic phase transition at finite magnetic field, below which the magnetic ordering is AFM, in a magnetic unit cell including at least two formula units, possibly with a more complex noncollinear magnetic structure that has not been considered here. Above the critical magnetic field, we expect the system to adopt the collinear *udu* FiM structure, with a single-formula-unit magnetic cell. We note that the degree of Mn/Fe antisite disorder, which may in turn have an effect on the magnetic properties, is not currently well characterized in our samples. We leave this as a topic of future investigation.

In conclusion, the new polar and magnetic Mn_2FeWO_6 prepared at HPT crystallizes in the corundum-based Ni_3TeO_6-type structure as established by electron and synchrotron X-ray diffraction. The asymmetric structure of Mn_2FeWO_6, directly evidenced by second-harmonic generation, is consistent with a large spontaneous polarization. The crystal structure and X-ray near-edge absorption spectroscopy analyses indicate formal oxidation states of Mn^{2+} (d^5, high spin (HS)), Fe^{2+} (d^6, HS) and W^{6+} (d^0). Complicated magnetic properties are observed in this *d*-electron-rich HS system. At low applied field (≤1 T) near 70 K, an AFM order is observed, which is suppressed with increasing magnetic field. Below ≈30 K, a first-order magnetic field-induced phase transition appears to a larger moment ferrimagnetic (FiM in the DFT calculations) state with a hysteresis of 4 T (7 to 3 T), which generates double-hysteresis loops in the isothermal magnetization curves. The hysteresis shrinks with increasing temperature and leads to a second-order transition near 30 K, which persists up to 70 K.

First-principles calculations confirm the structural parameters and oxidation states, and without cell doubling, they predict a FiM ground-state *udu*, with the Mn2 moments antiparallel to both Mn1 and Fe moments along the *c*-axis. The *udu* magnetic structure is insulating with a bandgap of 1.83 eV and the spontaneous polarization (P_S) is calculated to be 67.8 μC cm^{-2}, but the optimal switching path leads to a metallic intermediate structure, which hinders the polarization reversal. First-principles calculations also find an *udu–udd* double cell even lower in energy than the *udu* single-formula-unit structure, by 13 meV/f.u. Transitions between the single-formula-unit *udu* and the double-cell *udu–udd* give a likely explanation for the magnetic double-hysteresis loop.

Experimental Section

Details of the experimental and theoretical section are shown in the Supporting Information. Further details of the crystal structure investigation(s) may be obtained from the Fachinformationszentrum Karlsruhe, 76344 Eggenstein-Leopoldshafen (Germany), on quoting the depository number CSD-428616.

Supporting Information

Supporting Information is available from the Wiley Online Library or from the author.

Acknowledgements

This work was supported by the NSF-DMR-0966829 and DOD-VV911NF-12–1–0172 grants. Use of the National Synchrotron Light Source, Brookhaven National Laboratory was supported by the DOE BES (DE-AC02–98CH10886). M.Y. and D.V. are supported by the ONRN00014–12–1–1035 grant. H.A. and V.G. acknowledge support from the National Science Foundation grant numbers DMR-0820404 and DMR-1210588. C.Q.J. and W.M.L. are supported by NSF & MOST of China through research projects. The authors thank Jean Hanley at the Lamont-Doherty Earth Observatory in Columbia University for making the high-pressure assemblies, Dr. Juliane Gross at the American Museum of Natural History in New York City for the assistance of microprobe analyses.

Received: November 16, 2014
Revised: January 15, 2015
Published online: February 11, 2015

[1] R. Mathieu, S. A. Ivanov, G. V. Bazuev, M. Hudl, P. Lazor, I. V. Solovyev, P. Nordblad, *Appl. Phys. Lett.* **2011**, *98*, 202505.
[2] M.-R. Li, P. W. Stephens, M. Retuerto, T. Sarkar, C. P. Grams, J. Hemberger, M. C. Croft, D. Walker, M. Greenblatt, *J. Am. Chem. Soc.* **2014**, *136*, 8508.
[3] M.-R. Li, D. Walker, M. Retuerto, T. Sarkar, J. Hadermann, P. W. Stephens, M. Croft, A. Ignatov, C. P. Grams, J. Hemberger, I. Nowik, P. S. Halasyamani, T. T. Tran, S. Mukherjee, T. S. Dasgupta, M. Greenblatt, *Angew. Chem. Int. Ed.* **2013**, *52*, 8406.
[4] Y. S. Oh, S. Artyukhin, J. J. Yang, V. Zapf, J. W. Kim, D. Vanderbilt, S.-W. Cheong, *Nat. Commun.* **2014**, *5*.
[5] S. A. Ivanov, R. Mathieu, P. Nordblad, R. Tellgren, C. Ritter, E. Politova, G. Kaleva, A. Mosunov, S. Stefanovich, M. Weil, *Chem. Mater.* **2013**, *25*, 935.
[6] M.-R. Li, M. Retuerto, D. Walker, T. Sarkar, P. W. Stephens, S. Mukherjee, T. S. Dasgupta, J. P. Hodges, M. Croft, C. P. Grams, J. Hemberger, J. Sánchez-Benítez, A. Huq, F. O. Saouma, J. I. Jang, M. Greenblatt, *Angew. Chem. Int. Ed.* **2014**, *53*, 10774.
[7] A. A. Belik, T. Furubayashi, H. Yusa, E. Takayama-Muromachi, *J. Am. Chem. Soc.* **2011**, *133*, 9405.
[8] P. M. Woodward, A. W. Sleight, L.-S. Du, C. P. Grey, *J. Solid State Chem.* **1999**, *147*, 99.
[9] C. A. Hoel, J. M. G. Amores, E. Morán, M. A. Álario-Franco, J.-F. Gaillard, K. R. Poeppelmeier, *J. Am. Chem. Soc.* **2010**, *132*, 16479.
[10] R. Mathieu, S. A. Ivanov, I. V. Solovyev, G. V. Bazuev, P. Anil Kumar, P. Lazor, P. Nordblad, *Phys. Rev. B* **2013**, *87*, 014408.
[11] J. Choisnet, A. Rulmont, P. Tarte, *J. Solid State Chem.* **1988**, *75*, 124.
[12] M. W. Lufaso, P. M. Woodward, *Acta Crystallogr. Sec. B* **2001**, *57*, 725.
[13] D. L. Bish, S. A. Howard, *J. Appl. Crystallogr.* **1988**, *21*, 86.
[14] I. D. Brown, R. D. Shannon, *Acta Crystallogr. Sect. A* **1973**, *29*, 266.
[15] C. Lefevre, F. Roulland, A. Thomasson, C. Meny, F. Porcher, G. André, N. Viart, *J. Phys. Chem. C* **2013**, *117*, 14832.
[16] Y. Inaguma, M. Yoshida, T. Katsumata, *J. Am. Chem. Soc.* **2008**, *130*, 6704.
[17] J. Y. Son, G. Lee, M.-H. Jo, H. Kim, H. M. Jang, Y.-H. Shin, *J. Am. Chem. Soc.* **2009**, *131*, 8386.
[18] R. Hsu, E. N. Maslen, D. du Boulay, N. Ishizawa, *Acta Crystallogr. Sect. B* **1997**, *53*, 420.
[19] R. Shannon, *Acta Crystallogr. Sect. A* **1976**, *32*, 751.